CHINESE OPTICS LETTERS

Vol. 21, No. 1 | January 2023

InAs/GaAs quantum dot laterally coupled distributed feedback lasers at 1.3 μm

Wenfu Yu (于文富)[1,2], Xuyi Zhao (赵旭熠)[1,2], Shixian Han (韩实现)[1,2], Antian Du (杜安天)[3], Ruotao Liu (刘若涛)[1,2], Chunfang Cao (曹春芳)[1], Jinyi Yan (严进一)[1], Jin Yang (杨 锦)[1], Hua Huang (黄 华)[1], Hailong Wang (王海龙)[3], and Qian Gong (龚 谦)[1,2*]

[1] Key Laboratory of Terahertz Solid State Technology, Shanghai Institute of Microsystem and Information Technology, Chinese Academy of Sciences, Shanghai 200050, China

[2] Center of Materials Science and Optoelectronics Engineering, University of Chinese Academy of Sciences, Beijing 100049, China

[3] School of Physics and Physical Engineering, Shandong Provincial Key Laboratory of Laser Polarization and Information Technology, Qufu Normal University, Qufu 273165, China

*Corresponding author: qgong@mail.sim.ac.cn

Received April 13, 2022 | Accepted July 15, 2022 | Posted Online September 21, 2022

We report the InAs/GaAs quantum dot laterally coupled distributed feedback (LC-DFB) lasers operating at room temperature in the wavelength range of 1.31 μm. First-order chromium Bragg gratings were fabricated alongside the ridge waveguide to obtain the maximum coupling coefficient with the optical field. Stable continuous-wave single-frequency operation has been achieved with output power above 5 mW/facet and side mode suppression ratio exceeding 52 dB. Moreover, a single chip integrating three LC-DFB lasers was tentatively explored. The three LC-DFB lasers on the chip can operate in single mode at room temperature, covering the wavelength span of 35.6 nm.

Keywords: InAs; quantum dot; laterally coupled distributed feedback laser.
DOI: 10.3788/COL202321.011402

1. Introduction

High performance, reliable, and low cost semiconductor lasers are crucial for applications in the field of optical communication[1]. While single-channel optical interconnects can operate with electrically pumped Fabry–Perot lasers, distributed-feedback (DFB) lasers, which provide single-longitudinal-mode emission with a narrow spectrum line width, are indispensable for wavelength division multiplexing systems[2]. A number of advantages of the GaAs-based InAs quantum dot (QD) laser diodes operating in the 1310 nm wavelength region have been found over the commercial InP-based III–V quantum well (QW) lasers, such as low threshold current density, high quantum efficiency (QE), and high temperature stability[3–6]. Moreover, a very important advantage of QD lasers is that the QDs active region has been proved to be much less sensitive to crystal defects than in the conventional QW structures due to effective three-dimensional carrier localization[7]. Thus, InAs QDs are desirable to be utilized for the active region of silicon-based lasers[8,9]. The InAs/InGaAs QDs DFB laser becomes very important in the development of silicon-based photonics. Although the electrically pumped DFB laser using InAs/GaAs QD gain material epitaxially grown on silicon was reported by Wang *et al.*[10], there is still very little research effort on InAs QD DFB lasers[11,12].

In this work, we report the fabrication and characterization of 1.31 μm GaAs-based QD laterally coupled DFB (LC-DFB) lasers by employing the first-order Cr gratings. Excellent single-longitudinal-mode characteristics with a high side mode suppression ratio (SMSR) above 52 dB have been achieved. With an injection current of 300 mA, the LC-DFB laser emits up to 5 mW per facet.

2. Experimental Procedure

The laser structure was grown on 4 in. n-type GaAs (001) substrates by a solid source molecular beam epitaxy system equipped with an As cracker. The grown structure was started with a 500 nm GaAs buffer layer deposited at 720°C after native oxide desorption. Then, a 1.5 μm n-doped $Al_{0.4}Ga_{0.6}As$ cladding layer and 20 periods of 2 nm/2 nm $Al_{0.4}Ga_{0.6}As$/GaAs superlattices (SLs) waveguide layer were grown, followed by a five-fold stacked InAs/InGaAs dot-in-well (DWELL) structure. The SLs are used here to lower the barrier for carrier transport and to reduce the serial resistance. The DWELL structure

consists of 2 nm $In_{0.15}Ga_{0.85}As$, 2.2 nm monolayer InAs, and 6 nm $In_{0.15}Ga_{0.85}As$ covering the QD layer. GaAs barrier layers with thickness of 50 nm were grown to separate the five DWELL structures. After that, 20 periods of 2 nm/2 nm AlAs/GaAs SLs waveguide layers and 1.5 μm p-doped $Al_{0.4}Ga_{0.6}As$ cladding layers were grown, following the active region. Finally, a 300 nm P+-GaAs contact layer completed the growth. The growth temperature was 720°C for GaAs, 610°C for In-containing layers, and 760°C for $Al_{0.4}Ga_{0.6}As$ layers.

Narrow ridge waveguide DFB lasers were fabricated with ridge width of 3 μm. The ridge structures were defined by optical lithography followed by chlorine-based inductively coupled plasma reactive ion etching. The etching was stopped when the depth reaches the active region. Then, Cr gratings were fabricated alongside the ridge waveguide by electron beam lithography and lift-off process. A 200-nm-thick Si_3N_4 layer was deposited by plasma-enhanced chemical vapor deposition for insulation and ridge side wall passivation. Ti/Pt/Au metal layers were deposited for the top n-contact. The substrate was thinned down to about 120 μm. Au/Ge/Ni/Au metal contacts were applied for the back. The design of our LC-DFB lasers was based on coupled-wave theory, and the first-order grating is used[13–15]. Figure 1 shows the high resolution scanning electron microscope (SEM) images, where the cleaved facet of the laser is shown in Fig. 1(a), and the ridge top is shown in Fig. 1(b).

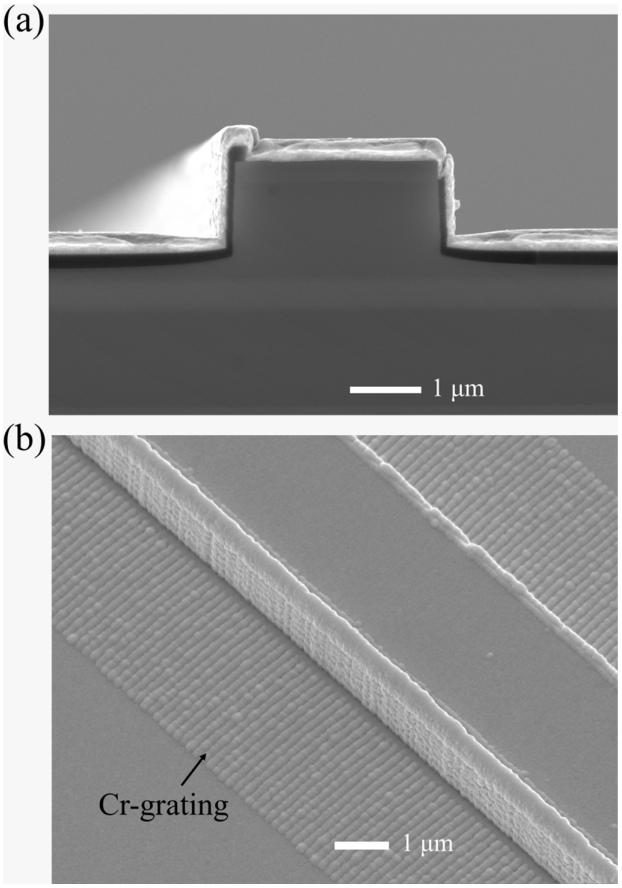

Fig. 1. SEM image of the LC-DFB laser. (a) Cross-section view. (b) Top view.

Uniform Cr gratings with periods of 196.5 nm are clearly shown, which are covered by a silicon nitride isolation layer and the top electrode metal films. According to the coupled-wave theory, the coupling coefficient is given by[16,17]

$$\kappa = \frac{|n_2^2 - n_1^2|}{n_{\text{eff}}\lambda}\frac{\sin(\pi m \Lambda_1/\Lambda)}{m}\Gamma_{\text{grating}},$$

where n_2 and n_1 are the refractive indices of the dielectric layer and Cr gratings, respectively, n_{eff} is the effective refractive index, λ is the wavelength in vacuum, m is the grating order, first-order ($m = 1$) is used here, Λ_1 and Λ are the width of the Cr grating line and the grating period, respectively, and Γ_{grating} is the ratio of optical field intensity in the grating region to the overall region. The period of Cr grating Λ is calculated by $\Lambda = m\lambda/2n_{\text{eff}}$. Duty cycle is defined as $\gamma = \Lambda_1/\Lambda$, which strongly affects the coupling coefficient κ. In experiment, the duty cycle value of about 40% was used, while the grating period was 196.5 nm.

3. Result and Discussion

Laser diodes with cavity length of 4 mm were cleaved and mounted epi-side up on copper heat sinks by In soldering. Both facets were left uncoated. Narrow ridge lasers were measured in continuous-wave (CW) mode. The output power was measured by an integrating sphere InGaAs photodiode power sensor S145C from Thorlabs. For CW mode, a current and temperature controller ITC4020 from Thorlabs was used for current injection and heat sink temperature control. The device operating temperature was monitored by a resistance temperature detector PT100 mounted alongside the copper heatsink. An IS-50R Fourier transform infrared spectrometer and an OSA20 spectrum analyzer were used to record the lasing spectra.

The CW mode current-voltage-power (*I-V-P*) characteristics of an LC-DFB laser with 4-mm-long cavity and 3.0-μm-wide ridge are shown in Fig. 2(a). The laser has a threshold of 207 mA at 20°C, corresponding to a threshold current density of 1.72 kA/cm^2, and an output power of 5 mW per facet at 300 mA was recorded. It is worth noting that there is an output power kink point when the input current is 235 mA, which is likely caused by mode hopping. As shown in Fig. 2(b), the light emitting wavelength has a relatively large shift when the current

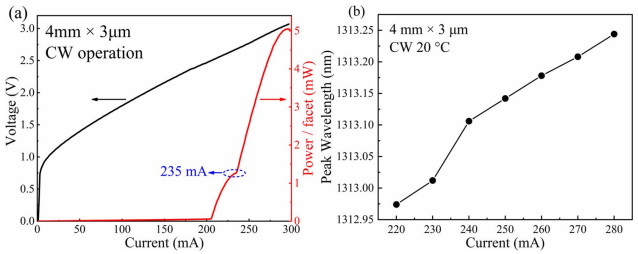

Fig. 2. (a) *I-V-P* characteristic of the LC-DFB laser in CW mode at 20°C. (b) The relationship between peak wavelength and current from 220 mA to 280 mA of the LC-DFB laser.

rises from 230 mA to 240 mA, indicating an occurrence of mode hopping. The gain and spatial refractive index coefficient are affected by the recombination of carriers[18], which may result in mode hopping when their changes are large enough.

The laser diode was systematically characterized in the temperature range of 10°C–30°C. Characteristic temperature T_0 was calculated as 45 K under CW mode, as shown in Fig. 3(a). Furthermore, from the *I-P* data, the slope efficiency of the laser was obtained, as well as the external QE. The QE is calculated by $\eta_{\text{ext}} = \frac{2q\lambda}{hc}\frac{\Delta p}{\Delta I}$, with h the Planck constant, c the speed of light, q the electron charge, λ the lasing wavelength, p the measured optical power, and I the injection current. The temperature dependent external QE of the laser is shown in Fig. 3(b), where it is evident that a maximum external QE reaches 19% at 20°C in the temperature range of 10°C–30°C. This tendency is reasonable for LC-DFB lasers, where the overlap of the gain peak wavelength and the mode wavelength determined by the gratings plays a critical role. Maximum external QE was obtained at 20°C, indicating the best overlap was achieved. For operating temperatures varying away from 20°C, the overlap becomes worse, leading to a decrease in the external QE, as shown in Fig. 3(b). Note that there is still room for improvement in the device performance such as threshold current density, external QE, and characteristic temperature. One of the main factors that should be considered is the optical loss caused by the Cr gratings. In addition, the parasitic spontaneous electron-hole recombination in the regions outside the QDs and the presence of the excited states in QDs in addition to the ground state[19,20] may also play a role in the device operation.

Under CW operation, the lasing wavelength can be tuned by varying the injection current and operating temperature. Lasing spectra the LC-DFB laser collected at 20°C are shown in Fig. 4(a), with injection currents varying from 230 mA to 350 mA in steps of 10 mA. In this current range, it is found that the LC-DFB laser is running as mode-hop free with very high SMSR values. Figure 4(b) shows the dependence of operating wavelength and SMSR on the injection current at different temperatures in the range of 10°C–30°C. A wavelength window of 1311.5–1314.5 nm can be covered by the LC-DFB laser operating in single mode. The tuning rates of the lasing wavelength with current and temperature are 4.15 pm/mA and 0.12 nm/K,

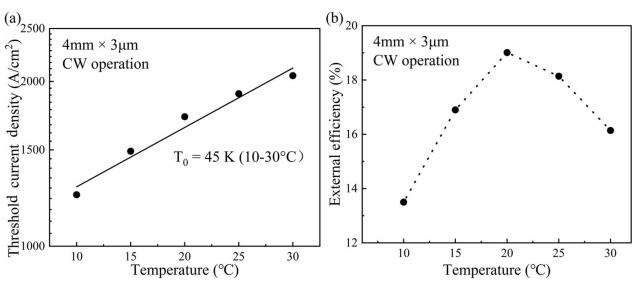

Fig. 3. (a) Characteristic temperature T_0 calculated under CW mode from 10°C to 30°C. (b) Variation of external efficiency calculated under CW mode from 10°C to 30°C.

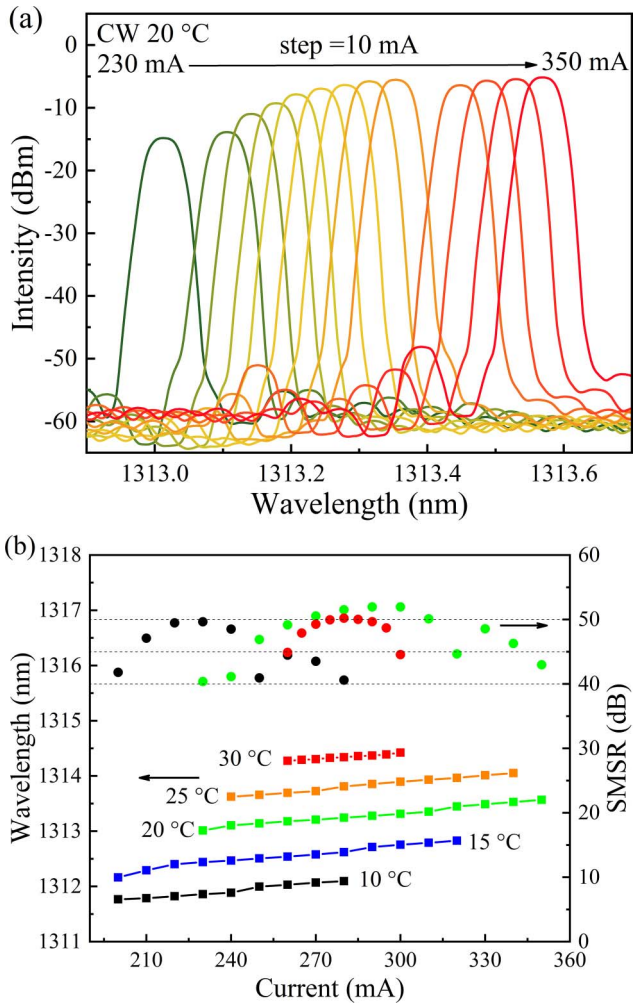

Fig. 4. (a) Spectra of the LC-DFB laser with injection current from 230 mA to 350 mA with a step of 10 mA at 20°C. (b) Variation of emission wavelength and SMSR versus current at different temperatures.

respectively. As shown in Fig. 4(b), for all the operating parameters (i.e., temperatures and injection currents), the SMSR over 40 dB were measured exclusively. The maximum SMSR has been obtained over 50 dB, indicating that the device has excellent single-mode operation performance[21]. Figure 5 shows a lasing spectrum of the LC-DFB laser, where the maximum SMSR of 52 dB has been achieved at 20°C with an injection current of 290 mA and a lasing wavelength of 1313.27 nm. This maximum SMSR value is better than that of most commercially available DFB lasers in this wavelength region[22]. The outstanding SMSR performance is attributed to the good match of mode wavelength selected by the Cr gratings and the peak of the gain profile.

InAs/GaAs QD gain material has a unique feature, i.e., its gain profile is much broader than that of the conventional QW structure. Thus, it is possible to fabricate a single chip that integrates several laser diodes covering a broad wavelength range, e.g., the wavelength span of the O-band four-wavelength coarse wavelength division multiplexing (CWDM) application (i.e., 60 nm).

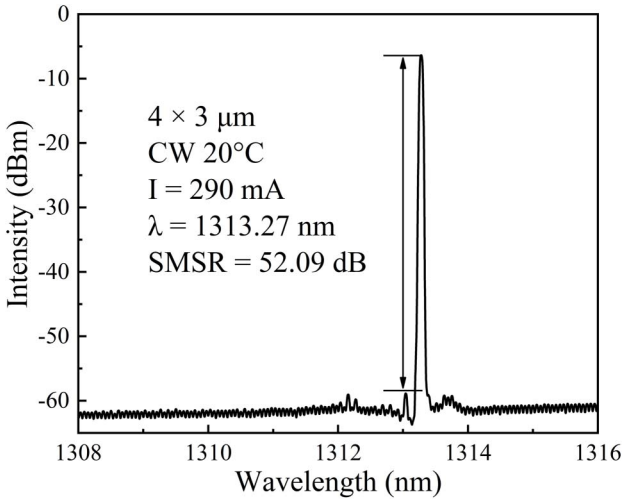

Fig. 5. Lasing spectrum of the LC-DFB laser with high SMSR ratio.

We tentatively explored the feasibility mentioned above by fabricating three LC-DFB lasers on a single chip. The operating wavelengths in the multi-laser chip were slightly different from the lasers discussed before, since a different epi-wafer was used for this purpose with gain peak located at shorter wavelength. As shown in Fig. 6, three operating wavelengths are achieved in a single chip integrating three LC-DFB lasers, while the wavelengths were determined by different periods of the gratings. The laser spectra were measured using a Fourier transform infrared spectrometer, in which a liquid-nitrogen cooled InSb detector and a CaF_2 beam splitter were used. It is found that a wavelength region of 35.6 nm can be covered by the LC-DFB lasers integrated in a single chip. This wavelength region can be further extended by optimization of the QD structure design and growth in order to cover the 60 nm wavelength span. Therefore, the QD LC-DFB lasers have significant potential in the CWDM applications, where only a single chip integrating four LC-DFB lasers is needed to provide a light source for four channels.

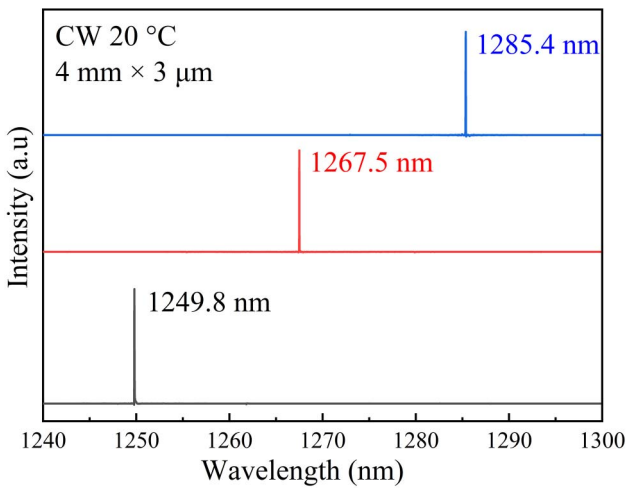

Fig. 6. Spectra of the LC-DFB laser arrays in CW mode at 20°C.

4. Conclusion

In conclusion, we have demonstrated high performance GaAs-based InAs QDs LC-DFB lasers employing Cr metal gratings along the ridge side. Single-mode operation was achieved in CW mode at room temperature, with SMSR in the range of 40–52 dB and output power of 5 mW. Wavelength tuning properties were characterized, and the tuning rates of 4.15 pm/mA and 0.12 nm/K were obtained, respectively. Moreover, a single chip integrating three LC-DFB lasers was tentatively explored. It is found that each LC-DFB laser on the chip can operate in single mode at room temperature. The chip was able to cover the wavelength span of 35.6 nm, showing significant potential in the CWDM applications.

Acknowledgement

This work was supported by the National Key Research and Development Program of China (No. 2021YFB2800500).

References

1. B. Dagens, J. Renaudier, R. Brenot, A. Accard, F. van Dijk, D. Make, O. Le Gouezigou, J.-G. Provost, F. Poingt, J. Landreau, O. Drisse, E. Derouin, B. Rousseau, F. Pommereau, and G.-H. Duan, "Recent advances on InAs/InP quantum dash based semiconductor lasers and optical amplifiers operating at 1.55 μm," IEEE J. Sel. Top. Quantum Electron. **13**, 111 (2007).
2. C. P. Joseph, *Fiber Optic Communications* (Pearson Prentice Hall, 2005).
3. Q. Li, X. Wang, Z. Zhang, H. Chen, Y. Huang, C. Hou, J. Wang, R. Zhang, J. Ning, J. Min, and C. Zheng, "Development of modulation p-doped 1310 nm InAs/GaAs quantum dot laser materials and ultrashort cavity Fabry-Perot and distributed-feedback laser diodes," ACS Photonics **5**, 1084 (2018).
4. G. Liu, A. Stintz, H. Li, K. Malloy, and L. Lester, "Extremely low room-temperature threshold current density diode lasers using InAs dots in $In_{0.15}Ga_{0.85}As$ quantum well," Electron. Lett. **35**, 1163 (1999).
5. M. Asada, Y. Miyamoto, and Y. Suematsu, "Gain and the threshold of three-dimensional quantum-box lasers," IEEE J. Quantum Electron. **22**, 1915 (1986).
6. O. B. Shchekin and D. G. Deppe, "1.3 μm InAs quantum dot laser with T_o = 161 K from 0 to 80°C," Appl. Phys. Lett. **80**, 3277 (2002).
7. Z. T. Mi, J. Yang, P. Bhattacharya, G. X. Qin, and Z. Q. Ma, "High-performance quantum dot lasers and integrated optoelectronics on Si," Proc. IEEE **97**, 1239 (2009).
8. K. Nishi, K. Takemasa, M. Sugawara, and Y. Arakawa, "Development of quantum dot lasers for data-com and silicon photonics applications," IEEE J. Sel. Top. Quantum Electron. **23**, 1901007 (2017).
9. A. Y. Liu, C. Zhang, J. Norman, A. Snyder, D. Lubyshev, J. M. Fastenau, A. W. K. Liu, A. C. Gossard, and J. E. Bowers, "High performance continuous wave 1.3 μm quantum dot lasers on silicon," Appl. Phys. Lett. **104**, 041104 (2014).
10. Y. Wang, S. Chen, Y. Yu, L. Zhou, L. Liu, C. Yang, M. Liao, M. Tang, Z. Liu, J. Wu, W. Li, I. Ross, A. J. Seeds, H. Liu, and S. Yu, "Monolithic quantum-dot distributed feedback laser array on silicon," Optica **5**, 528 (2018).
11. Y. Qiu and P. Gogna, "Laterally coupled InAs quantum dot distributed feedback lasers at 1.3 μm," in *IEEE-NANO* (2003), p. 414.
12. S. R. Jain, M. N. Sysak, G. Kurczveil, and J. E. Bowers, "Integrated hybrid silicon DFB laser-EAM array using quantum well intermixing," Opt. Express **19**, 13692 (2011).

13. M. J. Wallace, Q. Lu, W.-H. Guo, and J. F. Donegan, "Design optimization for semiconductor lasers with high-order surface gratings having multiple periods," J. Light. Technol. **36**, 5121 (2018).
14. C.-A. Yang, S.-W. Xie, Y. Zhang, J.-M. Shang, S.-S. Huang, Y. Yuan, F.-H. Shao, Y. Zhang, Y.-Q. Xu, and Z.-C. Niu, "High-power, high-spectral-purity GaSb-based laterally coupled distributed feedback lasers with metal gratings emitting at 2 μm," Appl. Phys. Lett. **114**, 021102 (2019).
15. H. Kogelnik and C. V. Shank, "Coupled-wave theory of distributed feedback lasers," J. Appl. Phys. **43**, 2327 (1972).
16. W. Streifer, D. Scifres, and R. Burnham, "Coupling coefficients for distributed feedback single- and double-heterostructure diode lasers," IEEE J. Quantum Elect. **11**, 867 (1975).
17. K. Papatryfonos, D. Saladukha, K. Merghem, S. Joshi, F. Lelarge, S. Bouchoule, D. Kazazis, S. Guilet, L. Le Gratiet, T. J. Ochalski, G. Huyet, A. Martinez, and A. Ramdane, "Laterally coupled distributed feedback lasers emitting at 2 μm with quantum dash active region and high-duty-cycle etched semiconductor gratings," J. Appl. Phys. **121**, 053101 (2017).
18. B. Dong, J. Duan, H. Huang, J. C. Norman, K. Nishi, K. Takemasa, M. Sugawara, J. E. Bowers, and F. Grillot, "Dynamic performance and reflection sensitivity of quantum dot distributed feedback lasers with large optical mismatch," Photonics. Res. **9**, 1550 (2021).
19. L. Jiang and L. V. Asryan, "Excited-state-mediated capture of carriers into the ground state and the saturation of optical power in quantum-dot lasers," IEEE Photon. Technol. Lett. **18**, 2611 (2006).
20. L. V. Asryan and R. A. Suris, "Spatial hole burning and multimode generation threshold in quantum-dot lasers," Appl. Phys. Lett. **74**, 1215 (1999).
21. J. Wang, C. Z. Sun, B. Xiong, Y. Luo, Z. B. Hao, Y. J. Han, L. Wang, H. T. Li, and J. D. Yu, "1.3 μm laterally coupled distributed feedback laser with high side mode suppression ratio and bandwidth," in *Asia Communications and Photonics Conference (ACPC)* (2019), paper T3D.3.
22. R. Millett, K. Dridi, A. Benhsaien, H. Schriemer, K. Hinzer, and T. Hall, "Fabrication-tolerant 1310 nm laterally coupled distributed feedback lasers with high side mode suppression ratios," Photonics Nanostruct. **9**, 111 (2011).